Biomed Microdevices (2008) 10:611–622
DOI 10.1007/s10544-008-9172-9

Nano-opto-mechanical characterization of neuron membrane mechanics under cellular growth and differentiation

Ashwini Gopal · Zhiquan Luo · Jae Young Lee · Karthik Kumar · Bin Li · Kazunori Hoshino · Christine Schmidt · Paul S. Ho · Xiaojing Zhang

Published online: 16 May 2008

Abstract We designed and fabricated silicon probe with nanophotonic force sensor to directly stimulate neurons (PC12) and measured its effect on neurite initiation and elongation. A single-layer pitch-variable diffractive nanogratings was fabricated on silicon nitride probe using e-beam lithography, reactive ion etching and wet-etching techniques. The nanogratings consist of flexure folding beams suspended between two parallel cantilevers of known stiffness. The probe displacement, therefore the force, can be measured through grating transmission spectrum. We measured the mechanical membrane characteristics of PC12 cells using the force sensors with displacement range of 10 μm and force sensitivity 8 μN/μm. Young's moduli of 425±30 Pa are measured with membrane deflection of 1% for PC12 cells cultured on polydimethylsiloxane (PDMS) substrate coated with collagen or laminin in Ham's F-12K medium. In a series of measurements, we have also observed stimulation of directed neurite contraction up to 6 μm on extended probing for a time period of 30 min. This method is applicable to measure central neurons mechanics under subtle tensions for studies on development and morphogenesis. The close synergy between the nano-photonic measurements and neurological verification can improve our understanding of the effect of external conditions on the mechanical properties of cells during growth and differentiation.

Keywords Mechanotransduction · Cytomechanics · PC12 · Cell membrane · Growth · Differentiation · Nanogratings · Micro-electro-mechanical systems (MEMS) · Force sensor

A. Gopal · K. Kumar · K. Hoshino · X. Zhang (✉)
Department of Biomedical Engineering,
The University of Texas at Austin,
1 University Station, ENS 12,
Austin, TX 78712-0238, USA
e-mail: John.Zhang@engr.utexas.edu

Z. Luo · B. Li · P. S. Ho
Department of Mechanical Engineering,
University of Texas at Austin,
Austin, TX 78758, USA

J. Y. Lee · C. Schmidt
Department of Chemical Engineering,
University of Texas at Austin,
Austin, TX 78712, USA

1 Introduction

Neuronal studies are among the most fundamental building blocks of modern biology and medicine. Neurons establish axons and dendrites, the morphology of which determines the number and type of inputs they receive (Moore and Jan et al. 2002). It has been proposed that environment- and activity-dependent structural remodeling are critical cellular basis of learning and memory (Matsuzaki and Honkura et al. 2004). Neuronal shape and the complex pattern of connections in the nervous system depend on both progressive and regressive processes such as axonal elongation and axonal elimination (Purves and Lichtman 1980; Cowan, and Fawcett et al. 1984). The growth cone behavior that are involved in the generation of these neuronal cytoarchitecuture are apparently regulated in quite specific ways of extrinsic factors such as chemical gradient (in particular calcium; Kater and Mattson et al. 1988), and neurotrophic factor (Mitchison and Kirschner 1988). In particular, sensory neurons and PC12 cells also show clear evidence of solid, elastic behaviors below the tension threshold required for

growth, like springs at low tension levels (Dennerll 1988; Lamoureux and Zheng et al. 1992).

Axonal development of neurons is intimately dependent on applied mechanical tension (Bray 1984; Zheng and Lamoureux et al. 1991). Local 3-D cell growth microenvironment and size-dependant mechanical stimulations can have profound impacts on the reliability of regenerated nerves. Various techniques have been employed to understand cell membrane interaction with its external environment. Micropipette aspiration is a technique that employs a microneedle with a diameter of 1–10 μm for manipulating cells. The aspiration length varies with the applied pressure that in turn helps to determine the rigidity of the cellular membrane (Hochmuth 2000). Optical tweezers is an instrument used to optically attach particles to the cellular membrane and manipulate the complex over precisely defined distance to estimate the stiffness of the cell (Berns 1998; Guck and Ananthakrishnan et al. 2001). Magnetic twisting cytometry is a method that uses 4–5 um diameter magnetic bead which is bound to the cell coated with an extracellular matrix protein sensitive to target receptors. The cell displacement under external magnetic field twisting can be used to characterize cellular mechanics (Bausch and Ziemann et al. 1998). In addition, mechanical and fluidic membrane stretching are other techniques used to observe cells cultured on flexible substrates. The substrate is cyclically deformed where by the cells bound to the substrate are stretched (DePaola and Davies et al. 1999; You and Cowin et al. 2001; Basso and Heersche 2002). It has been observed that cell stiffness is sensitive to the substrate to which it is adhered to. Cells attached to the surface of a substrate via extracellular matrix can result in functional changes of the receptors present in the cell. Cells attempt to match the stiffness with that of the underlying substrate by altering the organization of the cytoskeleton (Discher and Janmey et al. 2005).

Many methods employed thus far are still limited by measurement range, resolution, and device-cell coupling for minimal invasive measurements (Bao and Suresh 2003). For neurons typically of small size (diameter less than 15 μm), irregular shape and fragile membranes (10–1,000 Pa), new tools are needed to quantify the membrane properties, especially the elastic modulus, and to reveal the cellular responses to mechanical stimulations. Further considerations are also needed on the compatibility of probes with materials and media in which biologically relevant studies are performed. Development of the probes would be such that they do not damage the cell and can be functional in a cell culture media such that cells are not removed from their growth environment. Atomic force microscope (AFM) cantilever, a well established technique to deform a single cell, is used to measure and map the stiffness of the cell that is generated across the cell surface (Mathur and Truskey et al. 2000). These probes have been designed to work on proteins and the size of the tip being really small for that particular application. Recent advancements in microfabricated multi-layer grating photonics (Hane and Endo et al. 2002; Kim and Barbastathis 2006; Zhang and Scott et al. 2006) enable non-destructive sensing and microscopy of single cells with high resolution.

In this paper, we demonstrate the integration of nanoscale one dimensional (1D) photonic grating, on MEMS cantilever to probe neurons during growth to investigate neuronal cell mechanics and impact on cellular differentiation and growth due to probing of cells. The advancement in micro-optical–biological interface design (Zhang and Chen et al. 2005) opens the window to observe and manipulate cells (typically on the order of 10–15 μm) with high resolution in liquid media. Here, we present single-layer pitch-variable diffractive nanogratings on silicon nitride probe to investigate membrane mechanics and stress of PC12 cells.

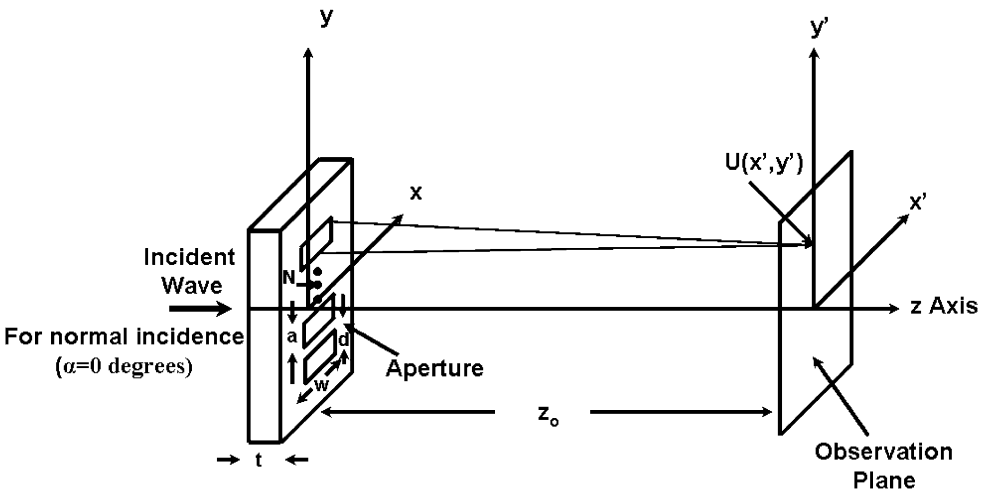

Fig. 1 Geometry for Fraunhofer diffraction of a phase grating

2 Principles of operation

2.1 Nanograting design and analysis

We implemented a binary phase transmissive grating design for its superior diffraction efficiency. For an electromagnetic wave passing through an aperture and imaged on a screen, the Fresnel number is defined as: $F = \frac{a^2}{z_o \lambda}$, where λ is wavelength of the wave, a is the characteristic size of the aperture, and z_o is the distance of the screen from the aperture. As shown in Fig. 1, the diffraction characteristics of this grating are analyzed using Fraunhofer diffraction principle (Goodman 2005) where the Fraunhofer diffraction equation is given by:

$$U\left(x^{'}, y^{'}\right) = e^{jkz_o} e^{j\frac{k}{2z_o}(x'2+y'2)} \frac{1}{j\lambda z_o} \Im(T_A(x,y))_{fx=\frac{x'}{\lambda z_o}, fy=\frac{y'}{\lambda z_o}} \quad (1)$$

The transfer function of the structure is:

$$T_A(x,y) = e^{i\phi o} \mathrm{rect}\left(\frac{x}{w}\right) \mathrm{rect}\left(\frac{y}{a}\right) \Theta \sum_{j=0}^{N-1} \delta(y - jd) \quad (2)$$

Where $T_A(x',y')$ is the transfer function of the grating structure, $e^{i\phi o}$ is the phase term that is present in the transmission phase grating, Θ represents convolution of the system, w is the aperture in the x-direction and a is the aperture in the y-direction ($a=d-dg$), N is the number of grating periods under illumination and d is the pitch of the grating structure. In our studies, w is on the order of 150 μm, λ is the wavelength of illumination that is on the order of 635 nm and viewing distance z_o is around 15–20 cm; hence Fraunhofer diffraction ($F<<1$) is applicable for this system.

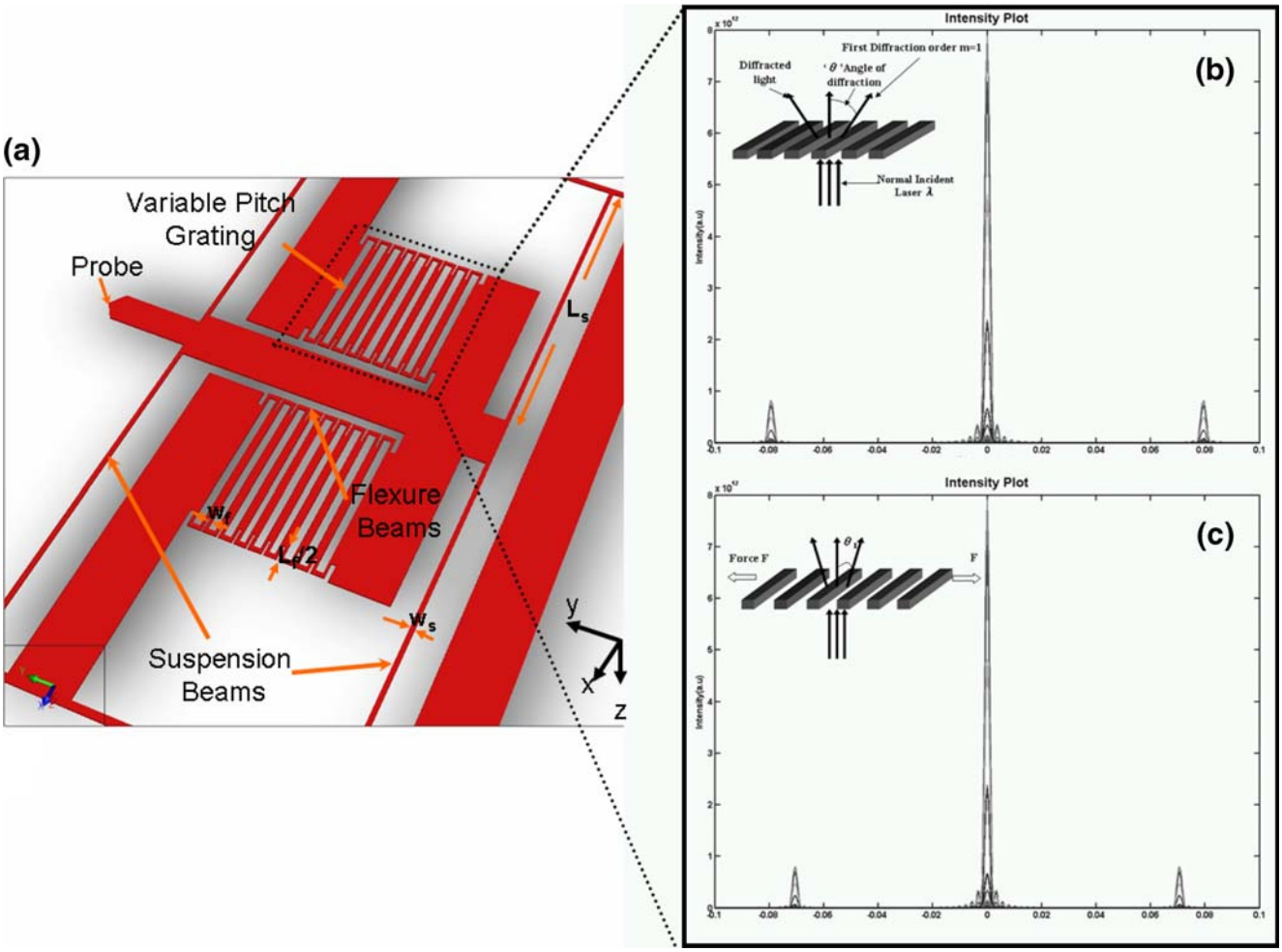

Fig. 2 Force sensor. (**a**) Schematic of nanograting force sensor. (**b**) Principle of operation of nanogratings force sensor under no load condition. (**c**) When a force is applied to the grating a change in pitch of the grating is observed; diffraction angle changes by force loading. Table 3: Device parameters for the nanograting structure

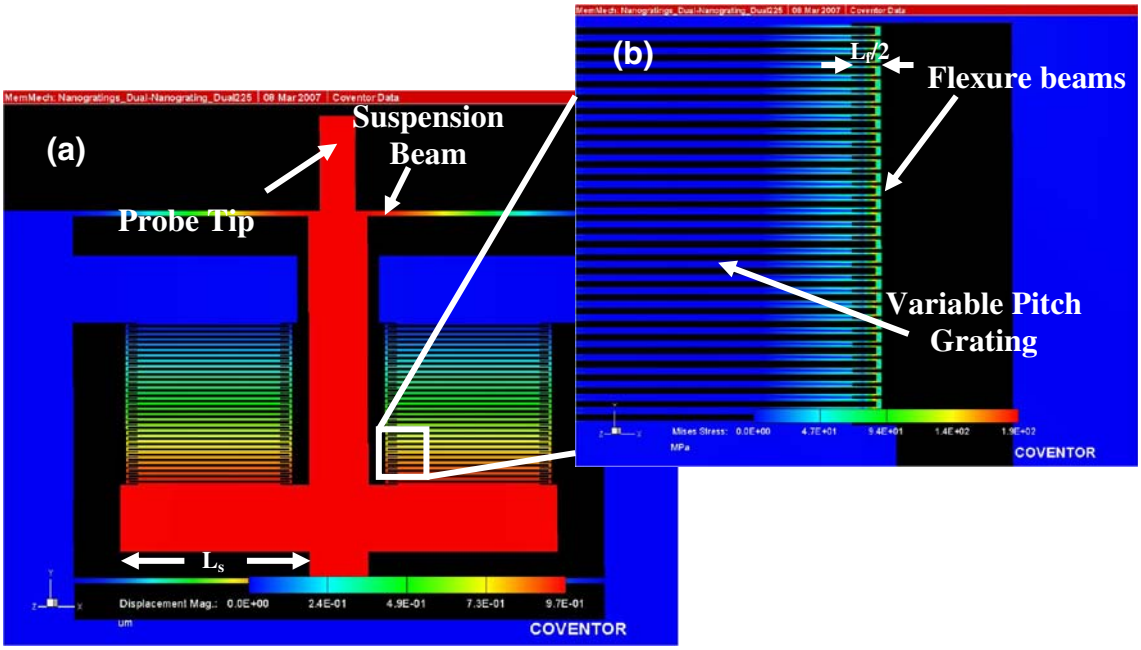

Fig. 3 Stress analysis of nanograting layer. (**a**) Sensor displacement (in microns) distribution using FEM analysis. (**b**) Stress (in mega Pascal) present only on the flexure folding junctions supporting the gratings. This shows that significant probe tip translation can be present while maintaining the flatness of the grating readout

The phase-delay over the thickness t of the structure is ϕ_o:

$$\phi_0 = \frac{2\pi\Delta n t}{\lambda} \tag{3}$$

Where,

$$\Delta n = n_{\text{Grating}} - n_{\text{Culture}} \tag{4}$$

Where n is the refractive index of the medium, Δn is the change in refractive index from culture media (n_{Culture} for PBS solution=1.35) to grating material (n_{Grating} for silicon nitride=2.02) is calculated using equation.

Hence the far field amplitude $U(x, y)$ is given by:

$$U(x,y) = e^{jkz_o} e^{j\frac{k}{2z_o}(x'2+y'2)} e^{-\frac{\pi dy}{\lambda z_o}} \frac{1}{j\lambda z_o} w \sin c\left(w\frac{x'}{\lambda z_o}\right)(N)\frac{\sin c\left((N)*d\frac{y'}{\lambda z_o}\right)}{\sin c\left(d\frac{y'}{\lambda z_o}\right)} \left[d\sin c\left(d\frac{y'}{\lambda z_o}\right) + (d-dg)\left(e^{i\phi o}-1\right)\sin c(d-dg)\frac{y'}{\lambda z_o}\right]\Bigg] \tag{5}$$

Intensity of Fraunhofer diffraction pattern for the force sensor:

$$I = |U(x,y)|^2 = -\frac{A^2}{\lambda^2 z_o^2}\sin c^2\left(w\frac{x'}{\lambda z_o}\right)\frac{\sin c^2\left((N)*d\frac{y'}{\lambda z_o}\right)}{\sin c^2\left(d\frac{y'}{\lambda z_o}\right)} \left[\begin{array}{l}\left(d\sin c\left(d\frac{y'}{\lambda z_o}\right) + (d-dg)\sin c(d-dg)\frac{y'}{\lambda z_o}(\cos\phi_o - 1)\right)^2 \\ +\left((d-dg)\sin c(d-dg)\frac{y'}{\lambda z_o} * \sin\phi_o\right)\right)^2\end{array}\right] \tag{6}$$

Where I is the intensity of the Fraunhofer diffraction pattern, $U(x, y)$ is the far field amplitude, $k = \frac{2\pi}{\lambda}$ is the wavenumber, λ is the wavelength of illumination, N is the number of grating periods under illumination, ϕ_0 is the phase-delay over the thickness of one grating finger, dg is the width of each grating rule in the period of the grating, d is the pitch of the grating structure.

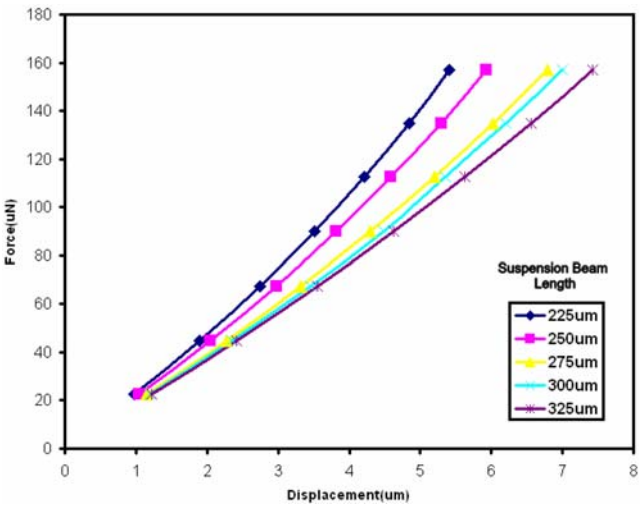

Fig. 4 Force versus displacement for different suspension beam lengths

Table 1 Variation of spring constant with respect to supporting beam length of the force sensor

Support beam length (μm)	Spring constant of the device[a] (N/m)
250	8.32
275	6.28
300	4.89
325	3.83
350	3.61

[a] K was calculated based on structure consisting of supporting beams and flexure beams together

The pitch variable phase gratings are operated in transmission. The diffraction equation under paraxial approximation is given by:

$$m\lambda = d(\sin\alpha + \sin\theta) \tag{7}$$

Where m is diffraction order, d is grating pitch, α is illumination angle, and θ is diffraction angle. Using Taylor series to expanding Eq. 7, the equation for normal illumination we get:

$$\frac{\Delta\theta}{\Delta d} = -\frac{m\lambda}{d^2\sqrt{1-\left(\frac{m\lambda}{d}\right)^2}} \tag{8}$$

Where the change in diffraction angle ($\Delta\theta$) per unit pitch (Δp) variation under normal illumination (α=0) is defined as the sensitivity of the sensor. Therefore, the sensitivity of the device can be greatly improved by reducing the critical feature size, d, of the grating. Improving sensitivity of the device implies that small changes in probe displacement will lead to large changes in diffraction pattern therefore even small displacements can be detected.

2.2 Sensor design

The force-sensing element presented here is a transmissive phase grating that is connected through nano-scale flexure beams, which is shown in Fig. 2. The grating is suspended by supporting beams and can be expanded by application of a load along the principal axis of the grating. This expansion changes the pitch of the grating, leading to a change in position of the diffraction orders (Fig. 2(b–c)). The nanograting is further integrated with a probe, both of which are suspended on cantilevers of known stiffness. The probe displacement, therefore the force, can be measured through tracking the position of the diffraction order (Table 3).

2.3 Mechanical stress, spring constant and eigen modes

Multilayer thin film microdevices are often fabricated through repetitive micro- or nanoscale processing including patterning, deposition and assembly. Intrinsic stresses are usually present which can distort the final micromachined

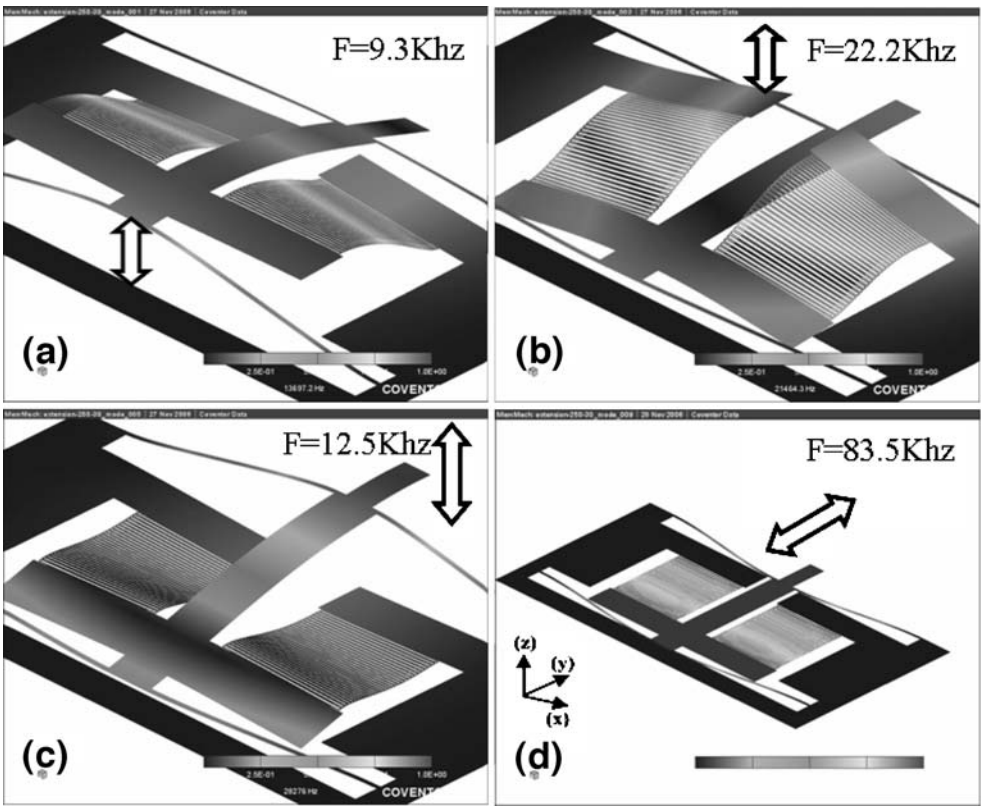

Fig. 5 Four eigen modes of operation of nanograting force sensor. (**a**) Up and down motion of the gratings. (**b**) Rotation about the X axis causing the buckling of the gratings. (**c**) Motion of the probe tip in the Z direction. (**d**) Y direction vibration which gives the required mode for this operation

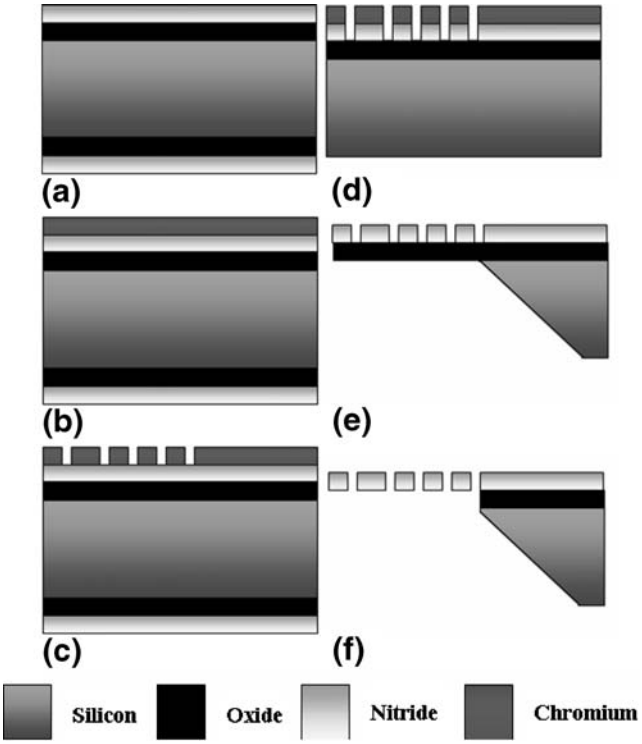

Fig. 6 Fabrication process of single layer nanograting force sensor. (**a**) Thermal oxidation of bare <100> silicon wafer. (**b**) Nitride LPCVD and chromium e-beam evaporation. (**c**) E-beam lithography and RIE of chromium (hard mask) layer. (**d**) Pattern transfer to nitride layer by RIE. (**e**) Dicing and TMAH etching of underlying silicon substrate. TMAH etch of the underlying substrate silicon. (**f**) Buffered oxide etch release

surfaces upon release. Two symmetric nanogratings are designed along each side of the probe (Fig. 3(a)) to provide mechanical balance and maximal optical surface area. With force (37.5 pN) applied to the probe tip, the amount of stress and the displacement across the grating layer was simulated using finite element method (FEM) Coventorware™. As shown in Fig. 3(a), the displacement of the sensor on application of force was on the order of 10 μm and in Fig. 3(b) the stress is present only on the folding junctions that hold the grating beams where in the stress is well under the yield stress level.

The spring constant k for various suspension beam lengths were simulated using finite element method (FEM) Coventorware™ (Fig. 4). To determine the effective spring constant (Senturia 2001, Nesterov and Brand 2004, 2005, 2006)) of the entire system contributed, there are two elements that contribute to the compliance of the device: the supporting beams which connect the suspended structure to the anchors, and the flexures which connect adjacent grating beams. The stiffness of the supporting beams is given by:

$$k_s = \frac{2Ew_s^3 t}{L_s^3} \tag{9}$$

Where k_s is the effective spring constant of the supporting beam, E is the Young's modulus of the material (for silicon nitride: 225 GPa), t is the thickness of the structure (750 nm), w_s is the width of the beam (4 μm), and L_s is the length of the supporting beam. The stiffness of the supporting beams on one side is estimated by considering two beams in parallel.

The stiffness of the flexure between two adjacent beams (one grating period) is estimated to be:

$$k_f = \frac{8Ew_f^3 t}{L_f^3} \tag{10}$$

Where k_f and L_f are the effective spring constant and the length of the flexure (10 μm) structure, respectively. w_f is the width of the flexure beam suspension (500 nm). The overall force constant of the nanograting sensor is a combination of k_s and k_f depending on the sensor dimension and geometry (Table 1).

The total spring constant of the device is given by:

$$k_t = 2k_s + \text{number of flexure beams} \times k_f/2 \tag{11}$$

For linear operation within small probe displacement, the force can be determined by $F=kx$. Where F is the force that

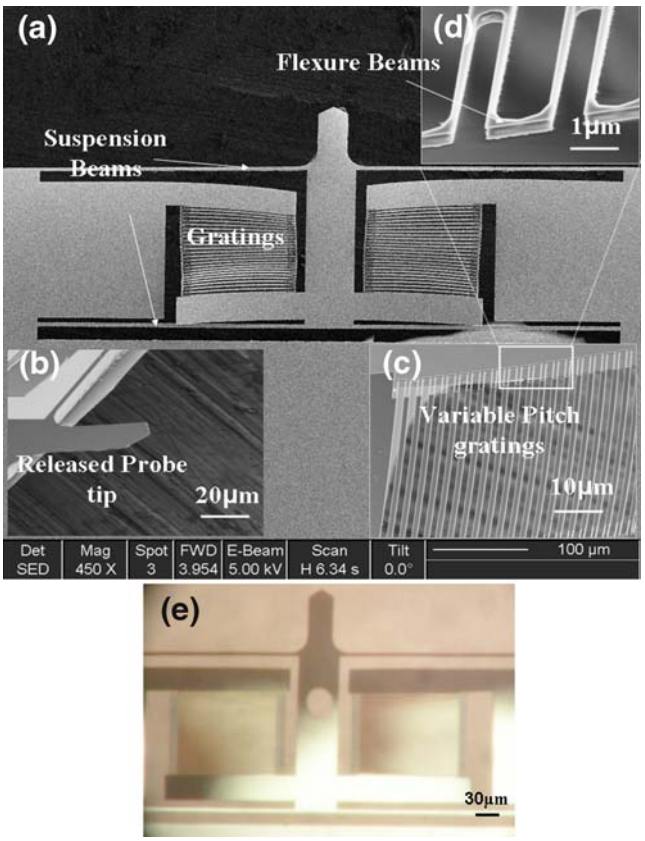

Fig. 7 Scanning electron micrographs (SEM) of the nanograting force sensor used in neuron membrane characterization. (**a**) Sensor overview, (**b**) released probe, (**c**) variable pitch gratings, (**d**) flexure folding beams and (**e**) optical micrograph of the nanograting force sensor indicating absence of deformation in the grating structure

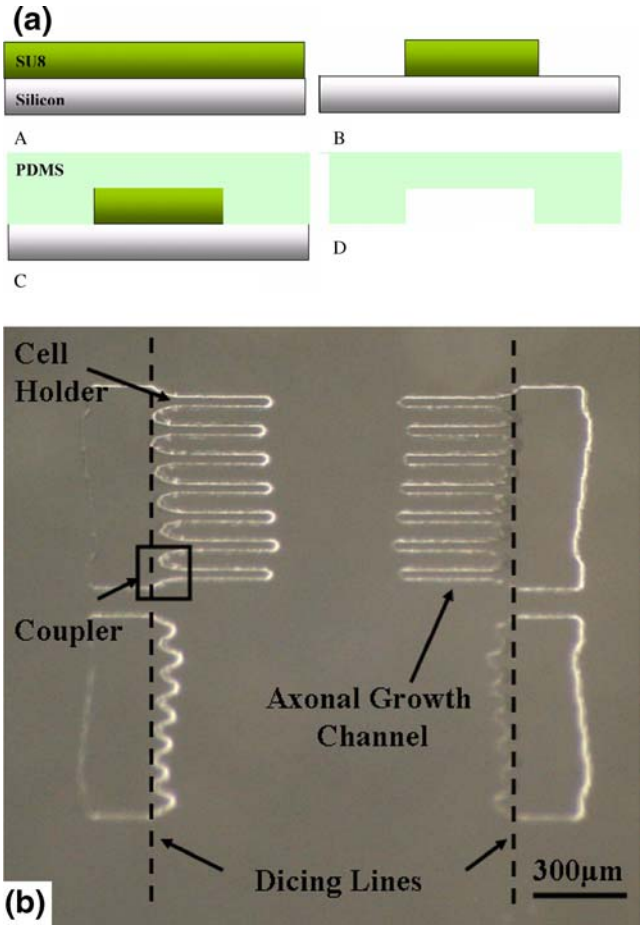

Fig. 8 PDMS cell holder. (**a**) Fabrication of PDMS cell holder. *A* Spin layer of SU9-2100 photoresist. *B* pattern and develop the master mold with UV through a dark field mask. *C* After baking PR, pour PDMS pre-polymer mixture over mold. *D* Place in oven and cure the polymer, and peel PDMS off the mold. (**b**) micro-fabricated PDMS neuron cell holder with coupler to force probe

is applied, k is the spring constant of the device and x is the displacement of the device. The force sensor can be treated as a linear spring–mass–dashpot system. Therefore the dynamic properties can be studied through eigen function analysis. Eigen modes under mechanical vibration were simulated using CoventorWare™ (Fig. 5). Eight fundamental modes were observed. Lower order modes had vibration present along the *Z*-axis that is greatly reduced by increasing the thickness. Only the *Y*-vibration modes are used for stress/strain measurements.

3 Device fabrication

As shown in Fig. 6, the fabrication of nanograting force probe described previously in (Gopal and Luo et al. 2007) begins with the deposition of 750 nm of silicon nitride device layer over 1000 nm of thermally oxidized <100> silicon wafer. Silicon nitride is transparent in the ultra violet wavelength region and hence can be used as a phase grating. Chromium (Cr) layer of 30 nm thickness is deposited over silicon nitride and is patterned using electron-beam lithography (EBL). A positive e-beam resist ZEP520-A is used for EBL. In EBL writing, the structure is aligned parallel to the <110> crystallographic direction of the silicon substrate. The sensor structure pattern is transferred from the e-beam resist to the Cr layer by reactive ion etching (RIE) process. Chrome acts as a hard mask during RIE to transfer the structure pattern into nitride layer. Nitride layer is partially etched and the device is placed in 25% TMAH solution held at 90°C to undercut the substrate until the device is completely released. Oxide layer is removed by buffered oxide etchant leaving the released nitride layer behind. During the tetra-methyl-ammonium-hydroxide (TMAH) etching process, the chromium layer is etched completely leaving behind silicon nitride as a device layer. Scanning electron micrographs (SEM) of the fabricated nanograting force sensor are shown in Fig. 7. The appearing deformation of the grating in the SEM was caused by the electron beam incident on silicon nitride surface. Curling of the silicon nitride suspended film was observed on scanning the electron beam across the surface of the device. An optical micrograph of the structure shows no such deformation present in the device (Fig. 7(e)) prior to SEM.

We also fabricated poly-di-methyl-siloxane (PDMS) cell holder to culture and immobilize the neurons for measurements. Prior to photolithography the master wafer is

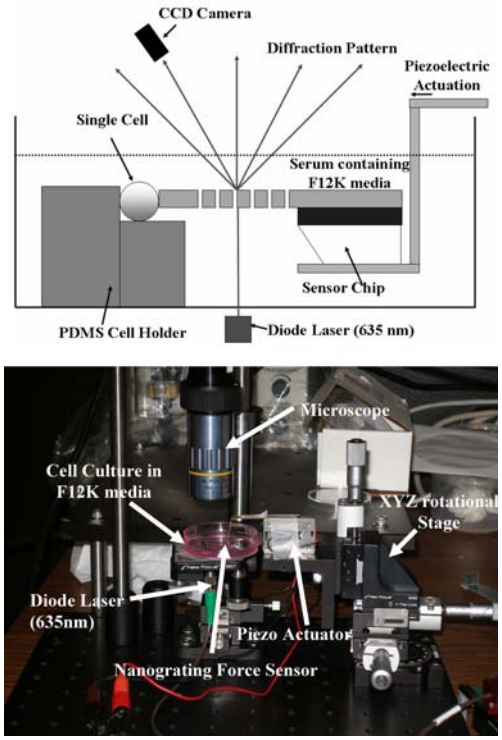

Fig. 9 Experimental setup for characterization of single neuron membrane mechanics

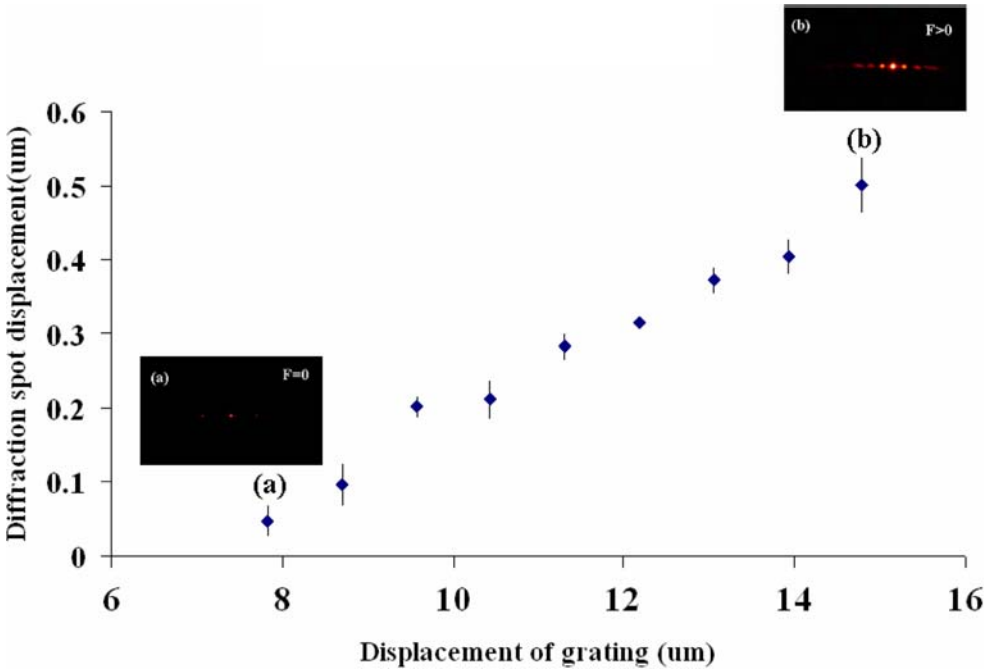

Fig. 10 Variation of diffraction spot with displacement of the force sensor. (**a**) Diffraction spots when no load is applied to the probe tip. (**b**) Variation of diffraction spots observed on application of force

cleaned using piranha cleaning method for a time span of 8 min. This wafer is then dipped into hydrofluoric acid (HF) for 20 s. The wafers are cleaned using deionized (DI) water and then dried using nitrogen. Clean wafers are then placed into an HMDS oven. Once the priming of the surface of the wafer is done using HMDS, the photoresist SU8 (Microchem Corp.) is spun for a time span of 50 s at 500 rpm (Fig. 8(a)).The wafer is then prebaked at 95°C for 20 min. Pattern is exposed onto the wafer for 95 s followed by post bake at 95°C for 45 min. The wafer was then developed using an SU8 developer and hard baked for 2 h. The channels are fabricated using polydimethylsiloxane (PDMS). A mixture of curing agent and PDMS in the ratio 1:10 are mixed and bubbles trapped in the PDMS are removed using a vacuum dessicator. This mixture of PDMS is then poured onto the master wafer containing the channels and then placed in the oven at 70°C for a time period of 4 h for curing. The channels are cut out of the mold using a scalpel, and pulled out using tweezers (Fig. 8(b)).

4 Experimental procedure and results

4.1 Materials and methods

PC12 an immortalized cell line derived from rat pheochromocytoma, can be induced to extend neurites with addition of nerve growth factor (NGF). Although there is no synaptic activity along the neurites of these cells, they serve as good models for neuron cells (Tischler and Greene 1976).

PC12 cells (American Type Tissue Collection) are routinely cultured in Ham's F-12K culture media (15% heat inactivated horse serum, 2.5% fetal bovine serum, 1% penicillin-streptomycin), in a humidified atmosphere maintained at 37°C, 5% CO_2 and passaged with a 0.05% trypsin and 0.01% EDTA solution every week. Priming of PC12 cells is done by culturing cells in medium containing 50 ng/ml of NGF.

Table 2 Measured angle of diffraction for normal illumination

Diffraction order (m)	1	2	3	4	5	6
Angle of diffraction (degrees)	9.1	18.5	28.4	39.4	52.5	72.2

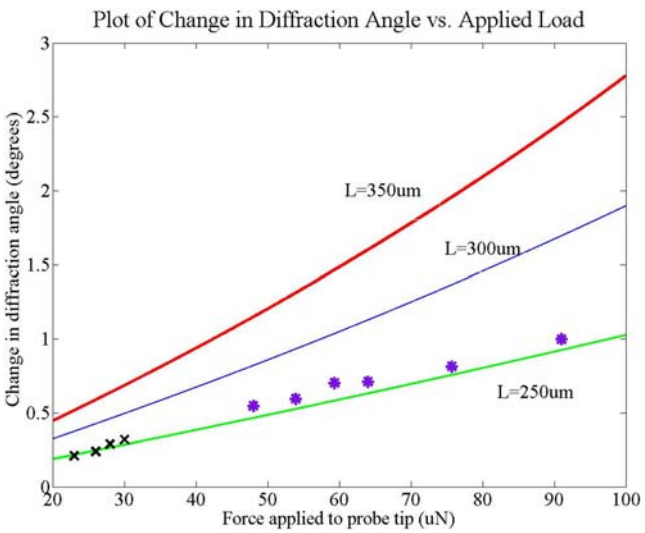

Fig. 11 Diffraction angle versus force: simulation (*solid lines*), calibration (*star*) and measurements (*cross*). Both calibration and measurements are for beam length of 250 μm

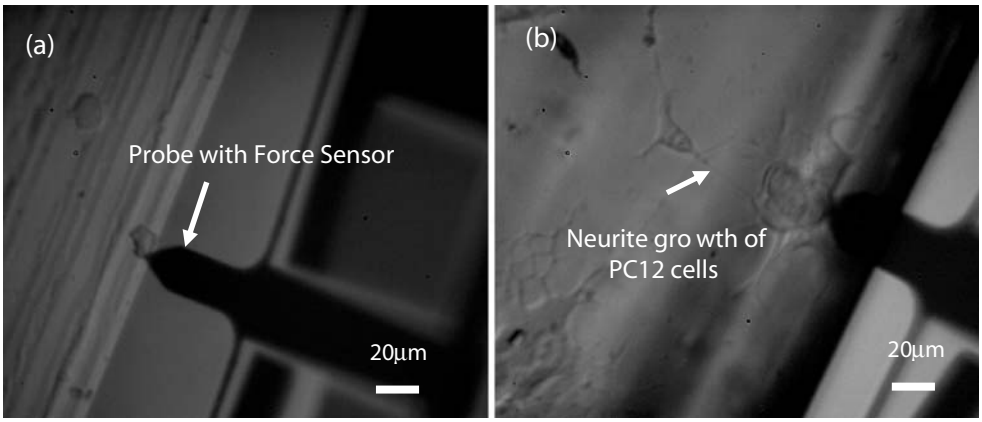

Fig. 12 Image of neurite growth characteristics of PC12 cells on (**a**) collagen coated substrate, with no neurite growth was observed, (**b**) collagen coated substrate treated with nerve growth factor, significant neurite growth was observed

PC12 cells are detached using Trypsin-EDTA solution (Life Technologies/Gibco BRL, Rockville, MD, USA), and washed with PBS buffer and media. The 2×10^4 cells per milliliter were seeded onto PDMS substrates that were placed in an F-12K culture media. Upon addition of Nerve growth factor (NGF) a well known morphogen for PC12 cells, branching neuron like process gradually attaining the phenotypic properties of sympathetic neurons was observed (S.D. Senturia Microsystem Design). We used murine 2.5S NGF (Promega) to study its effect on membrane stiffness of PC12 cells. In addition, its combinational effects with extra cellular matrix (ECM) components, such as collagen, were studied. Collagen: Rat tail collagen type I (Sigma), treating 1 mg/ml solution for 2 hours was used in the experiment.

4.2 Experimental setup and calibration

The experimental setup shown in Fig. 9 has a seamless integration of PDMS cell holders (1 cm×1 cm) with silicon nanograting probe that allowed biological measurements to be carried out in a liquid medium. The nanograting force sensor with the 50 μm long and 30 μm (Fig. 2) wide probe was attached to a piezoelectric actuator (Thorlabs), and subsequently placed in a liquid media (serum containing Ham's F-12K media) to probe the neurons. The sensor was illuminated with a 635 nm diode laser (Blue Sky Research), with the spot size (~100 μm diameter) covering the grating area of 120 μm×120 μm.

The probe displacement is measured by tracking the change of the diffraction order positions (Fig. 10). Diffraction spots were captured on a charged couple device (CCD) placed at 10° from normal placed at a distance of 15 cm from the force sensor. On illumination, the shift of diffraction angle indicated the amount of force applied to the cells. The first order diffraction spot (size on the order of 45 μm) was captured using a CCD (Basler Vision Technologies 659×480 pixels). In our experiments we implemented the use of the first order diffraction spot

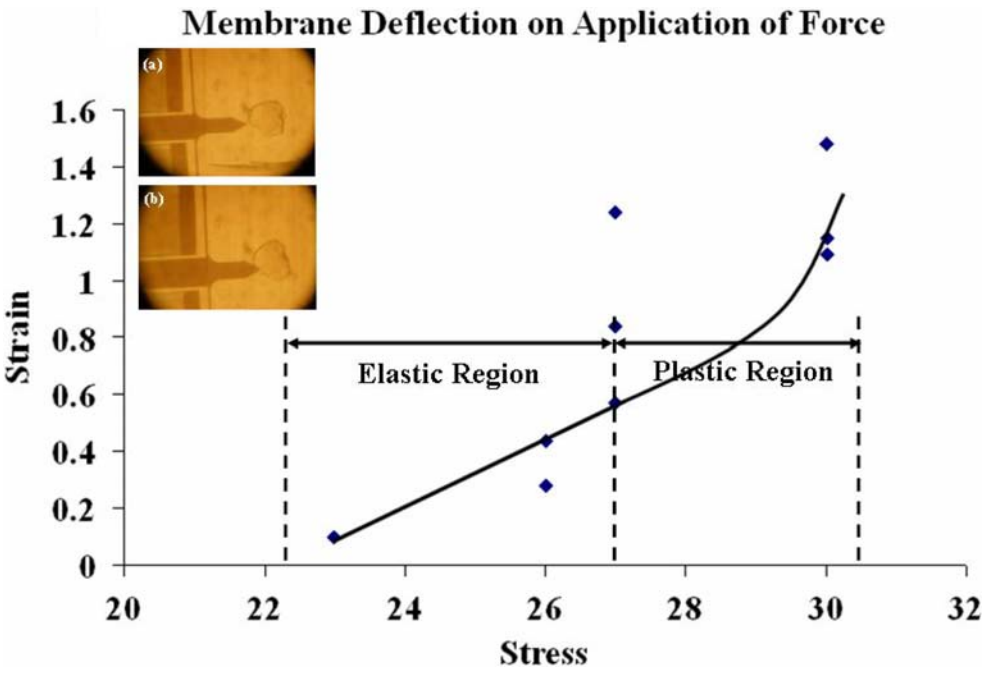

Fig. 13 Membrane deflection characterization of PC12 cells. *Embedded images* showing coupling of MEMS probe with the PC12 cells. (**a**) Ready to probe, with no membrane deflection, (**b**) membrane deflection by 5% after probing the PC12 cells

since intensity of the laser beam is concentrated in the lower order diffraction spots as seen from simulations previously. In the experiments the force sensor was aligned to the cell and was mounted on a piezoactuator. The sensor is in plane with the cell to ensure that there is perfect contact to the cell. The cell deformation on probing is simultaneously measured using an optical microscope. The cell deformation is given by the displacement of the cell membrane radially outwards on application of force to the surface of the cell. In this experiment the force response and the cell deformations were measured.

It was observed that the diffraction spots were measured with an error of ±10% (Table 2). Force sensor was calibrated by probing against a flat wall. The displacement of the sensor was predetermined by a calibrated piezo-transducer (Fig. 11). The variation of the diffraction spots fits very well with calculations using Snell's law and Fourier analysis.

4.3 Results and discussion

The method shown above was developed to study the cell mechanotransduction of PC12 cells due to external mechanical stimulation. The sensor was brought in contact with the cells laterally. The amount of force applied to the cell was read out using the diffraction spots captured using a CCD. Figure 11 shows that the measurement results fit well with theoretical simulations for 250 μm length beam. The change of the cell shape was recorded for a time period of 30 min with the sensor fixed at a particular position.

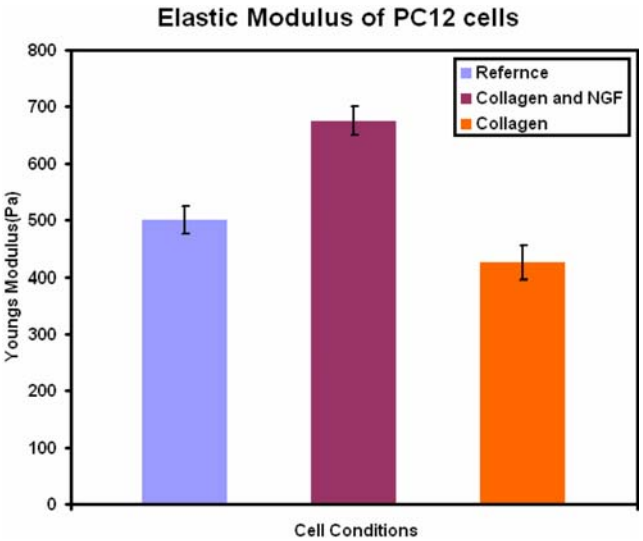

Fig. 14 Measured elastic modulus of PC12 cells under different substrate conditions. (The reference Young's modulus is adapted from (Radmacher and Fritz et al. 1996) for adhered platelets measured by AFM)

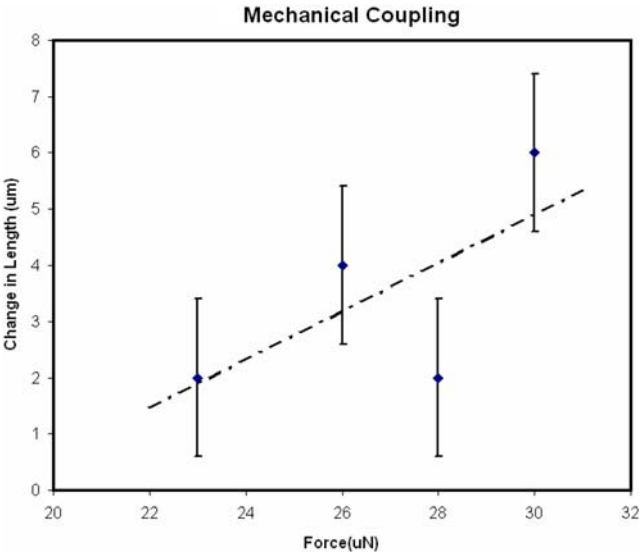

Fig. 15 Variation of dendrite length with application of force observed on multiple PC12 cells for a period of 30 min. Linear increase in dendrite length with application of force was observed

Figure 12(a) shows the probing of cells on collagen coated substrate with no NGF added to it. Figure 12(b) shows the probing of PC12 cells treated with NGF on collagen coated PDMS substrate. We deformed the membrane up to approximately 5% of its original shape to derive the elastic modulus of the cell (Fig. 13). As seen in Fig. 13 it was observed that when force was applied in the range of 20–27 μN the cell would return to the original shape. On applications of larger force it was observed that the deformation was irreversible. During the experiment it was observed that the cells deflected radially outwards on application of force. The elastic modulus of the cell was hence calculated using the following equation (Lur'e 1964) similar to deformable sphere:

$$E = \frac{\rho\sigma_{\mathrm{m}}}{2u_{\mathrm{r}}}\left(\frac{s-2}{s+1} - \frac{8-14s}{5+7s}\right) \tag{12}$$

Where E is the Young's Modulus, u_{r} is the radial deformation, s is the inverse of Possion's ratio, ρ is the

Table 3 Nanogratings device parameters

Device parameters	Values
Number of grating rules on each grating (N)	30
Grating area	120 μm×120 μm
Pitch of the grating (d)	4 μm
Suspension beam length (L_{s})	250 μm
Suspension beam width (w_{s})	4 μm
Thickness of the device (t)	750 nm
Flexure beam length (L_{f})	10 μm
Flexure beam width (w_{f})	500 nm
Elastic modulus of nitride layer	225 Gpa

radius, σ_m is the stress across the membrane and the Possion's ratio is 0.5 for biological membranes. In our case u_r, was determined by the change in radius of the cell observed on the screen.

It was estimated that the Young's modulus of the cells cultured on collagen substrate had an average modulus of 425±30 Pa, and those treated with NGF had a modulus of 675±25 Pa (Fig. 14). The experiment was conducted on 10–15 PC12 cells and the results were consistent. The PC 12 cells have a number of mechanical elements which comprise the cellular cytoskeleton and define its shape and locomotive abilities. This cytoskeleton is a filamentous network of several molecular components, including actin filaments, microtubules, and intermediate filaments. Actin filaments localize just beneath the cell membrane and in stress fibers that span the cell. Similarly, intermediate filaments and microtubules crisscross the cell, contributing to the cytoskeletal network that mechanically couples the cell membrane to the nucleus and points in between. The mechanisms as to how these components are able to provide mechanical stability to cells can be investigated using the method presented here. The results show that the presence of extensive cytoskeleton of the cells when treated with NGF as well as the extracellular matrix may have an impact on the elasticity of the cell. The presence of NGF increases the crosslinking inside the cell when compared to cells without NGF. We also found that an average force of 22±8 μN caused the neurite length to contract up to 6 μm (Fig. 15). The variation of neurite length on application of force show clear evidence of solid, elastic behaviors below the tension limit damaging the cell required for growth (Dennerll 1988; Lamoureux and Zheng et al. 1992), with high spatial–temporal force sensing resolution. These results suggest that mechanical tension is a critical factor in the development of neurites of a cell.

5 Conclusion

We designed and fabricated nanophotonic sensors integrated on a silicon probe to directly stimulate peripheral neurons, and measured its effect on neurite initiation and elongation.

The force sensor is comprised of a suspended diffraction grating structure whose pitch can be varied by application of a force (20 μN) on the tip of the probe. The diffraction grating is suspended on of nanometer-scale flexural beam. When a force (50 μN) is applied to the probe tip, the pitch of the diffraction grating is varied (by 0.5°). This variation can be sensed by illuminating the grating with a laser and viewing the change in position of the diffracted beam spot from the 'no-load' condition using a charged coupled device (CCD) camera. The sensitivity of the displacement sensor was determined to be 8 μm/μN by the stiffness of the beam structure by which the grating is suspended.

We numerically and experimentally calibrated the opto-mechanical response of single-layer pitch-variable diffractive nanogratings under various load conditions during the PC12 cells-probe interactions. Young's moduli of 425±30 Pa are measured with membrane deflection of 1% for PC12 cells cultured on PDMS substrate coated with collagen or laminin in Ham's F-12K medium. We have also observed stimulation of directed neurite contraction up to 6 μm on extended probing for a time period of 30 min. The close synergy between the nano-photonic measurement tools and cellular scale neurological verification can improve our understanding of the effect of the external conditions on the mechanical properties of cells during growth and differentiation. These findings will likely have a broad impact on understanding the role of neuron cytoskeleton in the pathology of nervous system disorders towards providing effective diagnosis and therapy.

Acknowledgments We would like to thank Microelectronics Research Center (MRC) and the Center for Nano and Molecular Science and Technology (CNM) at UT Austin for providing the microfabrication facilities. This study was supported in part by the National Science Foundation Nanoscale Exploratory Research Program (ECS-0609413).

References

G. Bao, S. Suresh, Nat. Mater. **2**, 715–725 (2003)
N. Basso, J.N.M. Heersche, Bone. **30**, 347–351 (2002)
A.R. Bausch, F. Ziemann et al., Biophys. J. **75**, 2038–2049 (1998)
M.W. Berns, Sci. Am. **278**, 52–7 (1998)
D. Bray, Dev. Biol. **102**, 379–389 (1984)
W.M. Cowan, J.W. Fawcett et al., Science. **225**, 1258–1265 (1984)
T.J. Dennerll, J. Cell. Biol. **107**, 665–674 (1988)
N. DePaola, P.F. Davies et al., Proc. Natl. Acad. Sci. U. S. A. **96**, 3154 (1999)
D.E. Discher, P. Janmey, et al., **310**, 1139–1143 (2005)
J.W. Goodman, Introduction to Fourier optics (Roberts & Co 2005)
A. Gopal, Z. Luo, et al., Solid-state sensors, actuators and microsystems conference, 2007. TRANSDUCERS 2007. International, 1239–1242 (2007)
J. Guck, R. Ananthakrishnan et al., Biophys. J. **81**, 767–784 (2001)
K. Hane, T. Endo et al., Sens Actuators: A. Physical. **97**, 139–146 (2002)
R.M. Hochmuth, J. Biomech. **33**, 15–22 (2000)
S.B. Kater, M.P. Mattson et al., Trends. Neurosci. **11**, 315–21 (1988)
WCSSG. Kim, G. Barbastathis, J. Microelectromechanical Syst. **15**, 763–769 (2006)
P. Lamoureux, J. Zheng et al., J. Cell. Biol. **118**, 655–661 (1992)
A.I. Lur'e Three-dimensional problems of the theory of elasticity (Interscience Publishers 1964)
A.B. Mathur, G.A. Truskey et al., Biophys. J. **78**, 1725–1735 (2000)
M. Matsuzaki, N. Honkura et al., Nature. **429**, 761–766 (2004)
T. Mitchison, M. Kirschner, Neuron. **1**, 761–72 (1988)

A.W. Moore, L.Y. Jan et al., Hamlet, a binary genetic switch between single- and multiple-dendrite neuron morphology Science **297**, 1355–1358 (2002)
V. Nesterov, U. Brand. The nonlinear mechanical and elastrical properties of silicon 3D micro probes, euspen. (2004)
V. Nesterov, U. Brand, J. Micromechanics Microengineering. **15**, 514–520 (2005)
V. Nesterov, U. Brand, J. Micromechanics Microengineering. **16**, 1116–1127 (2006)
D. Purves, J.W. Lichtman, Science. **210**, 153–157 (1980)
M. Radmacher, M. Fritz et al., Biophys. J. **70**, 556–567 (1996)
S.D. Senturia Microsystem Design (Kluwer Academic Publishers 2001)
A.S. Tischler, L. Greene, Proc. Natl. Acad. Sci. USA. **73**, 2424–2428 (1976)
L. You, S.C. Cowin et al., J. Biomech. **34**, 1375–1386 (2001)
X. Zhang, C.C. Chen et al., J. Microelectromechanical Syst. **14**, 1187–1197 (2005)
X. Zhang, M.P. Scott, et al., J. Microelectro. Mech. Syst. **15** (2006)
J. Zheng, P. Lamoureux et al., J. Neurosci. **11**, 1117–1125 (1991)